IJHSR
ijhighschoolresearch.org
RESEARCH ARTICLE

Hydrothermal Synthesis of Bracken-Derived Carbon Quantum Dots: A Sustainable Approach for Efficient Ferric Ion Detection

Rachel Jiwon Park, Hailey Jeongwon Park

Branksome Hall Asia, 234 Global edu-ro, Daejeong-eup, Seogwipo City, Jeju Special Self-Governing Province, 63644, Republic of Korea; rjpark2008@gmail.com

ABSTRACT: Biomass-derived carbon quantum dots (CQDs) have gained considerable attention as sustainable fluorescent materials due to their low toxicity, intense photoluminescence (PL), and facile synthesis. Among biomass sources, bracken, rich in polysaccharides, flavonoids, and organic acids, is a promising low-cost precursor for CQD production. In this study, we synthesize bracken-derived doped CQDs and explore their fluorescence (FL)-based sensing capability for ferric ions. Carbonized bracken powder was doped with sulfanilamide *via* a hydrothermal reaction, followed by purification of the resulting CQDs *via* a sequential filtration, centrifugation, and dialysis process. The CQDs were characterized *via* various instrumental analyses, such as FT-IR, UV–vis, and PL spectroscopy. In ion-sensing experiments, the effective adsorption of Fe^{3+} on CQDs induced pronounced fluorescent quenching, yielding a linear calibration curve in the range of 5–300 μM ($y = -0.35x + 174.14$). The limit of detection (LOD) and limit of quantification (LOQ) were calculated to be 8.52 and 25.80 μM, respectively. The results of the selectivity evaluation revealed that Fe^{3+} detection resulted in markedly greater fluorescent quenching than that of other metal ions. These results strongly demonstrate that bracken-derived CQDs function as effective and selective fluorescent probes for Fe^{3+} detection.

KEYWORDS: Environmental Engineering & Science, Green Chemistry, Carbon Quantum Dots, Metal Ion Adsorption, Fluorescence Sensing.

Introduction

In various environmental matrices, such as air, soil, and water, large quantities of heavy metals from industrial, agricultural, and urban activities can cause severe environmental pollution.[1,2] While pollutants in water or air are transported and diluted by flow, heavy metals introduced into the soil become strongly adsorbed and fixed to soil particles, particularly clay minerals and organic matter.[3] Furthermore, heavy metals entering aquatic systems are predominantly adsorbed onto particulate suspended matter rather than remaining in a dissolved state, eventually settling at the bottom of rivers and lakes. Unlike general organic chemicals or bacterial toxins, which can degrade over time or be detoxified by the immune system, heavy metals are elemental and thus non-biodegradable and persistent.[4] Among heavy metals, ferric ion (Fe^{3+}) can be introduced into water systems at concentrations significantly higher than natural levels due to industrial activities such as acid mine drainage, factory wastewater, and metal corrosion.[5] Because excessive Fe^{3+} disrupts aquatic ecosystems and contaminates drinking water sources, it is a critical target for detection in environmental monitoring networks. In addition, from a monitoring perspective, detecting Fe^{3+} is more practical for real-world environmental analysis, as Fe^{2+} is rapidly oxidized to Fe^{3+}—the final pollutant form—by atmospheric oxygen.[6]

The intense, tunable photoluminescence (PL) of quantum dots (QDs) enables them to serve as highly sensitive probes for detecting low concentrations of metal ions.[7,8] Among various types of QDs, carbon quantum dots (CQDs) have received increasing attention because they are low-cost, non-toxic, photostable, and can be synthesized through eco-friendly "green synthesis" routes.[9,10] Therefore, the development of CQD-based fluorescence (FL) sensors for heavy metal ion detection addresses critical environmental monitoring needs while offering early-warning systems to safeguard human and ecological health. Recently, biomass has emerged as an important renewable carbon source with broad applicability.[11] Biomass-derived CQDs have been extensively studied due to their intense PL, photostability, catalytic properties, and low toxicity, which render them suitable for applications in sensors, catalysis, and bioimaging.[12] Furthermore, they offer distinct environmental advantages by promoting resource recycling and sustainable material development. Biomass can be readily converted into CQDs *via* various synthetic methods, such as hydrothermal treatment, microwave-assisted synthesis, and pyrolytic carbonization.[13]

Bracken (scientific name: *Pteridium aquilinum*) is a perennial fern with a ubiquitous global distribution. While it has historical significance as a dietary source in some regions, it is frequently categorized as an invasive and opportunistic weed in many Western areas, often requiring intensive physical or chemical removal. From a material science perspective, utilizing this abundant and underutilized biomass as a carbon precursor offers a sustainable and value-added upcycling strategy.

Bracken is a particularly effective biomass precursor for CQD synthesis due to its complex lignocellulosic framework. It is rich in cellulose, lignin, and a variety of phenolic compounds, which serve as excellent carbon and oxygen sources. During the hydrothermal process, these organic polymers undergo dehydration and carbonization, facilitating the formation of stable sp^2-conjugated carbon domains that constitute the fluorescent

DOI: 10.36838/IJHSR816.129

core of the CQDs. Furthermore, the presence of intrinsic heteroatoms and diverse functional groups within the bracken matrix promotes self-doping and surface functionalization, potentially enhancing the optical properties of the resulting nanoparticles without the need for excessive external reagents. Consequently, transforming this widely available invasive species into functional CQDs represents a cost-effective and eco-friendly approach to environmental monitoring.

In environmental monitoring, rapid and accurate detection technologies are indispensable. Although conventional methods, such as electrochemical sensors and mass spectrometry, offer high precision, they are often constrained by high costs, the requirement for skilled personnel, and time-consuming procedures. To address these limitations, FL-based sensing systems have emerged as a promising alternative, characterized by operational simplicity and high sensitivity.[14] In this study, we synthesize N, S, and P-codoped CQDs utilizing carbonized bracken powder and sulfanilamide. Following the systematic characterization of their structural and optical properties, we evaluated their sensing performance, specifically targeting Fe^{3+}. Due to their paramagnetic nature and unfilled d-orbitals, Fe^{3+} ions act as effective electron acceptors and energy-transfer agents, serving as potent fluorescent quenchers. This interaction induces a pronounced quenching effect, thereby facilitating the highly sensitive and selective detection of Fe^{3+}.

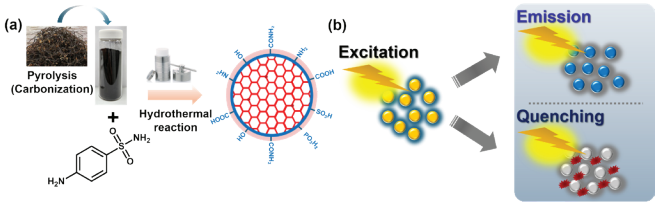

Figure 1: (a) Synthetic route of bracken-derived carbon quantum dots (CQDs) and (b) schematic illustration of PL emission (without any complex with ferric ions) and fluorescent quenching (by chelating with ferric ions) when CQD is photo-excited in an aqueous solution.

Methods

Materials:

Dried bracken, used as the carbon precursor, was sourced from Jeju, Republic of Korea, a region renowned for its abundant and high-quality wild bracken production. Sulfanilamide (Tokyo Chemical Industry Co., Ltd., Tokyo, Japan) was used as the N, S-dopant. Various metal salts were purchased to evaluate the ion-sensing selectivity of the CQDs: nickel(II) nitrate hexahydrate, sodium nitrate, and cobalt(II) nitrate hexahydrate, all obtained from Samjeon Pure Chemical Co., Ltd. (Pyeongtaek, Republic of Korea). Silver nitrate, magnesium sulfate, and potassium chloride were purchased from Duksan Pure Chemical Co., Ltd. (Ansan, Republic of Korea). Zinc nitrate hexahydrate, chromium nitrate nonahydrate, and barium nitrate were obtained from Daejung Chemicals & Metals Co., Ltd. (Siheung, Republic of Korea), while aluminum nitrate nonahydrate and iron nitrate nonahydrate were purchased from Junsei Chemical Co., Ltd. (Tokyo, Japan). All chemicals were used without further purification, and all organic solvents used were of ACS reagent grade.

Synthesis and Purification of Bracken-Derived CQDs:

Bracken-derived CQDs were synthesized as follows (Figure 1). Dried bracken was ground into a powder using a grinder. A 10 g sample of bracken powder was placed in a crucible and carbonized at 300 ˚C for 1 h in a furnace under an air atmosphere. The carbonized powder was finely ground and stored for further processing. The powder (3 g) was dispersed in 60 mL of distilled water, and a sulfanilamide solution (0.4 g) in 20 mL of ethanol was added. After stirring, the mixture was transferred to a hydrothermal reactor and heated at 200 ˚C for 4 h. The resulting solution was filtered through a 0.2 μm cellulose acetate membrane, and the filtrate was centrifuged at 13,500 rpm for 30 min using a Labogene mini centrifuge (Republic of Korea) to remove residual large particles. The supernatant was collected and dialyzed against distilled water for 24 h using a membrane with a molecular weight cut-off (MWCO) of 500 Da. During dialysis, the distilled water was replaced several times to ensure the removal of small impurities. The CQD solution was transferred from the dialysis tube into a round-bottom flask, and the solvent was removed using a rotary evaporator (IKA RV10, Germany). Finally, the CQD powder was collected from the round-bottom flask.

Structural and PL Characterization:

Surface functional groups and elemental composition were analyzed using Fourier transform infrared spectroscopy (FT-IR; FT/IR-6600, Jasco Co., Tokyo, Japan) and X-ray photoelectron spectroscopy (XPS; Nexsa, Thermo Fisher Scientific, Hillsboro, OR, USA), respectively. The crystalline structure was examined *via* X-ray diffraction (XRD; Panalytical Empyrean, Malvern Co., Malvern, Worcestershire, UK), while particle morphology and size distribution were characterized using transmission electron microscopy (TEM; Titan G2 ChemiSTEM, Thermo Fisher Scientific, Hillsboro, OR, USA). PL lifetime and absolute quantum yield (QY) were determined using a time-resolved fluorescent spectrometer (FLS-1000, Edinburgh Instruments, Livingston, Scotland, UK). The measurement was conducted using the absolute QY measurement method utilizing the equipped integrating sphere module. UV-vis absorption spectra were recorded with a Shimadzu UV-3600i Plus spectrophotometer (Kyoto, Japan), and PL emission spectra were obtained using a Jasco FP-6500 fluorometer (Tokyo, Japan).

Ferric Ion Detection:

Before the sensing experiments, FL stability was assessed under continuous 365 nm UV irradiation and across a pH range of 0.5–12.4. The effect of ionic strength on PL response was also investigated using varying KCl concentrations (0–1 M) to evaluate potential applicability in bioimaging. The Fe^{3+} sensing performance was examined by monitoring fluorescent quenching over a concentration range of 0–300 μM and calculating the detection sensitivity (limit of detection). Selectivity tests were performed using 0.5 mM solutions of interfering metal ions.

Results and Discussion

Structural Properties of Bracken-Derived CQDs:

The size and chemical structure of CQDs are critical factors in determining their fluorescent properties. As shown in the size distribution graphs (Figures 2a and 2b), dark grains of CQDs are well-dispersed, with an average particle size of approximately 9.30 nm. Given that this is larger than the typical size of CQDs (3–5 nm), this suggests that partial aggregation may have occurred. Moreover, as shown in Figure 2c, the CQDs display distinct lattice fringes across the entire particle area, indicating a graphitic-like crystalline structure. The d-spacing of the CQDs was measured to be 0.249 nm, corresponding to the (100) or (1120) plane (in-plane lattice of the hexagonal carbon ring in a graphene sheet).[15] In the XRD pattern, a broad peak is observed around 2θ = 21°, corresponding to a d-spacing of 0.42 nm. This indicates that the CQDs consist primarily of amorphous or turbostratic graphite components associated with the (002)-like plane, suggesting a disordered carbon framework. This structural characteristic may be attributed to the presence of surface functional groups and heteroatom doping, which will be further verified through FT-IR and XPS analyses in the following sections (Figure 3a).[16]

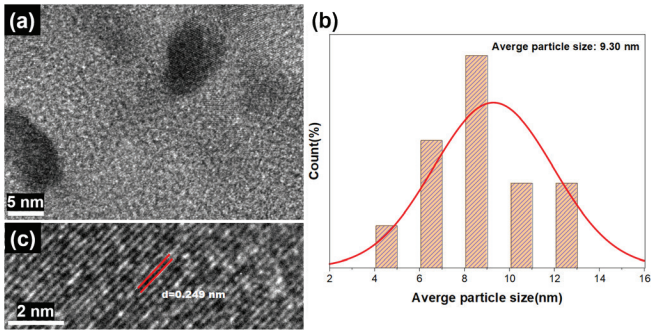

Figure 2: Morphology and structural characterization of the bracken-derived CQDs. (a) Transmission electron microscopy (TEM) image showing well-dispersed nanoparticles. (b) Particle size distribution histogram fitted with a Gaussian curve, indicating an average diameter of 9.30 nm. (c) High-resolution TEM (HRTEM) image displaying distinct lattice fringes with an interplanar spacing of 0.249 nm. TEM and HRTEM analyses of the bracken-derived CQDs show well-dispersed nanoparticles and lattice fringes.

The surface functional groups of the CQDs were further characterized by FT-IR spectroscopy. As shown in Figure 3b, a weak peak appears at 1640 cm^{-1} due to the stretching vibration of C=C bonds, which originate from the aromatic sp^2 (π-bonded) carbon domains within the CQD core. The absorption band at 3340 cm^{-1} is attributed to the overlapping vibrations of O–H and N–H functional groups.[17] Additionally, the bending vibrations corresponding to N–H and C–N groups at 1570 cm^{-1} confirm the presence of nitrogen doping.[18] Due to the sulfanilamide doping, symmetric and asymmetric stretching vibrations of SO_2 groups are observed at 1150 cm^{-1} and 1300 cm^{-1}, respectively.[19] Peaks at 1100 cm^{-1} and 1450 cm^{-1} indicate the formation of C–O–P and P=O functional groups on the surface of the CQDs.[20] These functional groups likely originate from inorganic phosphate present in the bracken, which may condense into pyrophosphate species or form phosphate ester bonds with hydroxyl and carboxyl groups during carbonization. Additionally, organic phosphate esters may decompose and dehydrate during the process, leading to the incorporation of P-doping sites on the CQD surface.

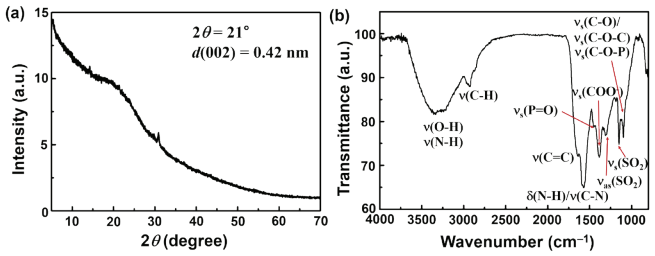

Figure 3: Spectroscopic characterization of the bracken-derived CQDs. (a) X-ray diffraction (XRD) pattern showing a broad diffraction peak centered at 2θ = 21°, corresponding to an interlayer spacing (d-spacing) of 0.42 nm. (b) FT-IR spectrum identifying surface functional groups. XRD analysis reveals an amorphous or turbostratic carbon structure, while FT-IR spectra confirm the presence of N, S, and P-containing functional groups.

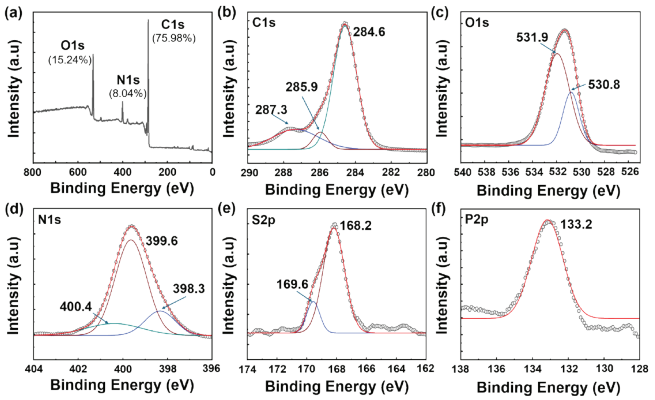

Figure 4: XPS analysis of the synthesized N, S, and P-codoped CQDs. (a) Full-scan survey spectrum showing the elemental composition. High-resolution spectra of (b) C 1s, (c) O 1s, (d) N 1s, (e) S 2p, and (f) P 2p. XPS analysis confirms successful N, S, and P codoping of the CQDs.

To further investigate these surface functional groups, the elemental composition and chemical structure of the N, S, and P-codoped CQDs were analyzed using XPS. As shown in Figure 4a, binding energy peaks corresponding to O1s, N1s, and C1s were observed at 545.0, 402.2, and 298.1 eV, respectively. Quantitative elemental analysis revealed that the CQDs contained 15.24 at% oxygen, 8.04 at% nitrogen, and 75.98 at% carbon. In addition, due to the introduction of dopants and the intrinsic components of bracken, small amounts of sulfur (0.59 at%) and phosphorus (0.14 at%) were incorporated into the CQDs.[21] In other words, the resulting CQDs feature intentional N, S-doping and natural P-enrichment, inherited from the intrinsic phosphorus content (~0.2% by dry weight) of the bracken precursor.[22] In the high-resolution spectra (Figures 4b and 4c), three major peaks for carbon were identified at 284.6 eV (C–C/C=C), 285.9 eV (C–N/C–O), and 287.3 eV (C=O), while the oxygen peaks were mainly associated with C=O (530.8 eV) and C–O– (531.9 eV) bonds. These results are consistent with the FT-IR analysis, confirming that the CQD surface is rich in hydrophilic groups, including hydroxyl and carboxyl moieties.

DOI: 10.36838/IJHSR816.129

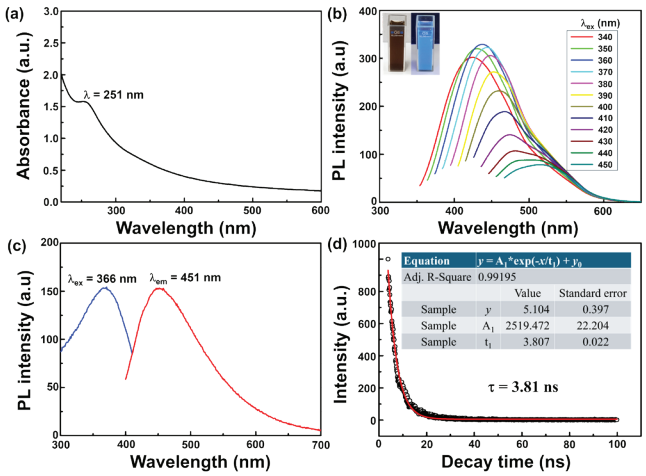

Figure 5: Optical properties of the bracken-derived CQDs. (a) UV–vis absorption spectrum showing a characteristic peak at 251 nm. (b) PL emission spectra were recorded under various excitation wavelengths from 340 to 450 nm. The inset displays photographs of the CQD solution under natural light (left) and 365 nm UV light (right). (c) PL excitation (blue line) and emission (red line) spectra, with maxima at 366 nm and 451 nm, respectively. (d) Time-resolved fluorescence decay profile fitted with a mono-exponential function, yielding an average lifetime (τ) of 3.81 ns. The CQDs exhibit a uniform radiative transition process with a peak emission at 450 nm.

Furthermore, the N1s spectrum (Figure 4d) clearly shows major peaks at 398.3 eV (pyridinic nitrogen), 399.6 eV (pyrrolic nitrogen), and 400.4 eV (graphitic nitrogen), indicating successful nitrogen doping as a key heteroatom. To investigate the minor dopants, the S2p and P2p spectra were analyzed (Figures 4e and 4f). Although present in trace amounts, distinct chemical states were observed. For sulfur, a peak corresponding to sulfoxide/sulfone (C–SO_x) was observed at 168.2 eV, while a sulfate ($–SO_4^{2-}$) peak appeared at 169.6 eV due to surface oxidation.[23] Additionally, the phosphorus signal showed a peak at 133.2 eV, attributed to P–O–C and P=O functional groups, which typically form during moderate-temperature synthesis (200–400 °C).

Optical Properties and Stability of CQDs:

An aqueous solution containing 0.1 mg/mL CQDs was used to investigate the optical properties of the CQDs. As shown in Figure 5a, the UV–vis absorption spectrum exhibits a single peak at 251 nm, which is typically attributed to the n–π* electronic transition of carbonyl (C=O) or nitroso (N=O) groups within the sp^3-hybridized domains of the CQDs.[24] In addition, the inset photographs in Figure 5b display the appearance of the CQD solution under natural light (left) and UV light (λ = 365 nm). While the aqueous solution appears dark brown under natural light, it exhibits strong blue photoluminescence (PL) under UV irradiation. Given the average particle size from the TEM images, the blue emission likely arises from abundant surface defects and functional groups formed by the carbon precursor and dopant, rather than quantum confinement. Furthermore, the large particles observed in the TEM images may be characteristic of carbon polymer dots (CPDs), consisting of aggregates of individual blue-emissive CQDs. As the excitation wavelength ($λ_{ex}$) is varied from 340 to 450 nm, the emission peaks shift from 420 to 520 nm (Figure 5b). The highest PL intensity was observed at an excitation wavelength of 360 nm. This characteristic behavior of CQDs is primarily determined by variations in particle size and the distribution of emission trap sites.[25]

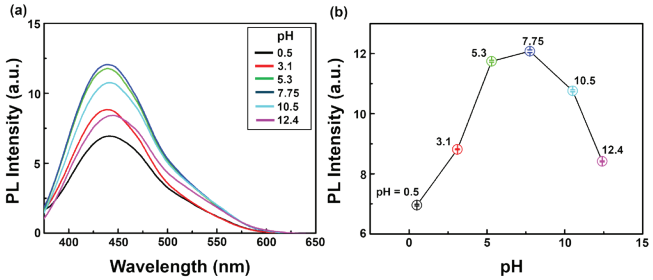

Figure 6: Effect of pH on the PL intensity of the bracken-derived CQDs. (a) PL emission spectra were recorded at different pH values ranging from 0.5 to 12.4. (b) Variation of the maximum PL intensity as a function of pH, indicating the pH-dependent fluorescence behavior. This result suggests that the PL intensity is stable near neutral pH but drops at extreme pH levels due to surface group changes.

To investigate the PL properties in more detail, PL excitation (PLE) and emission spectra were obtained. As shown in Figure 5c, the PLE spectrum exhibits an absorption peak at 366 nm, corresponding to electron transitions from the highest occupied molecular orbital (HOMO) to the lowest unoccupied molecular orbital (LUMO) within the π-orbitals (or sp^2 domains). Upon excitation at this wavelength, the maximum emission peak appears at 451 nm, with a full width at half maximum (FWHM) of approximately 125 nm. Furthermore, the fluorescence lifetime of the CQDs was determined to be 3.81 ns based on the FL decay profile measured at an excitation wavelength of 370 nm and an emission wavelength of 450 nm (Figure 5d). This single-exponential decay behavior indicates a relatively uniform radiative transition process in the CQDs.[26] In addition, the fluorescent QY under 370 nm UV excitation was measured to be 0.03% in an aqueous solution and 0.19% in a 1:1 (v/v) ethanol/distilled water mixture. The PL emission of these CQDs is attributed to the radiative recombination at passivated surface energy traps.[27]

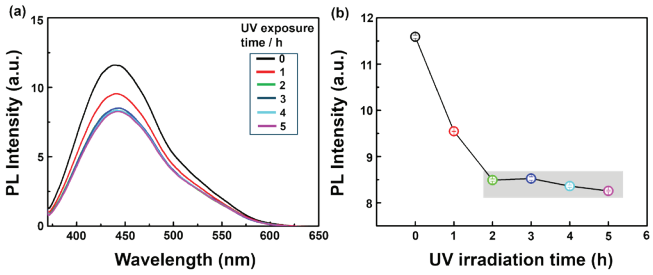

Figure 7: Photostability evaluation of the bracken-derived CQDs under continuous UV irradiation. (a) PL emission spectra recorded at 1-h intervals over a period of 5 h ($λ_{ex}$ = 365 nm). (b) Time-dependent variation of the PL intensity. The shaded region indicates the stabilization of PL emission after 2 h of UV irradiation. This result shows that the emission stabilized under prolonged UV irradiation, following the initial 2 h decline caused by UV degradation.

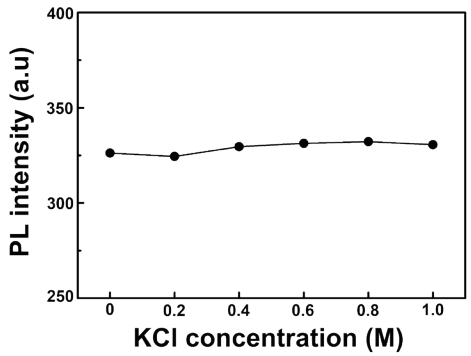

Figure 8: Stability analysis of CQDs (0.1 mg/ml) via fluorescence emission spectra under varying ionic strengths (0–1 M KCl).

To determine the optimal operating conditions for the sensor, the effect of pH on the PL intensity of the CQDs was investigated over a wide pH range (0.5–12.4). As shown in Figure 6a, the PL intensity shows a strong dependence on solution pH. The corresponding trend in Figure 6b clearly indicates that the PL emission reaches its maximum at pH 7.75 and remains relatively stable near neutral conditions (pH 5.3–7.75). However, a significant decrease in PL intensity is observed under strongly acidic (pH < 3) or alkaline (pH > 10) conditions. This phenomenon can be attributed to the protonation and deprotonation of the abundant surface functional groups (e.g., –COOH, –NH_2, –OH). In highly acidic environments, protonation of carboxyl and amino groups can induce CQD aggregation or alter their surface electronic states, leading to fluorescent quenching.[28] Conversely, under strongly basic conditions, the deprotonation of surface moieties can facilitate non-radiative electron recombination pathways, resulting in reduced emission. The high stability observed near neutral pH suggests that the synthesized CQDs are well-suited for environmental and biological applications that require physiological pH conditions.

Additionally, to evaluate the fluorescent stability of the CQDs, the emission intensity was measured at 1-h intervals over 5 h under continuous UV irradiation (λ_{ex} = 365 nm) (Figure 7a). Although the emission intensity decreased gradually over time, it retained 71.2% of its initial value. During the initial 2 h, the emission decreased significantly due to UV degradation; however, the emission stabilized upon prolonged UV irradiation (Figure 7b), demonstrating UV photostability. Therefore, the CQDs exhibit excellent long-term fluorescent stability and low susceptibility to degradation, indicating strong potential for practical applications. It is noteworthy that the fluorescence degradation occurred primarily during the initial 2 h. This initial drop can be attributed to the photo-oxidation or photobleaching of thermally unstable functional groups or surface defects on the CQDs.[29] However, after this "burn-in" period (0–2 h), the PL intensity reached a steady state (indicated by the grey shaded region), showing negligible further variations. This suggests that the core structure and stable surface passivation layers of the CQDs are robust against prolonged UV exposure. Consequently, despite the initial attenuation, the CQDs exhibit sufficient long-term photostability to serve as reliable fluorescent probes. Furthermore, the fluorescence intensity of CQDs was monitored in aqueous KCl solutions with various concentrations ranging from 0 to 1 M (Figure 8). Across the entire concentration range, the change in fluorescence intensity ($I_{PL,ave}$ = 329.1 ± 3.1 at λ_{ex} = 360 nm, λ_{em} = 436 nm) was negligible. This result indicates that the CQDs exhibit excellent stability even under high-salt conditions, suggesting their strong potential for various applications in complex and harsh environments.

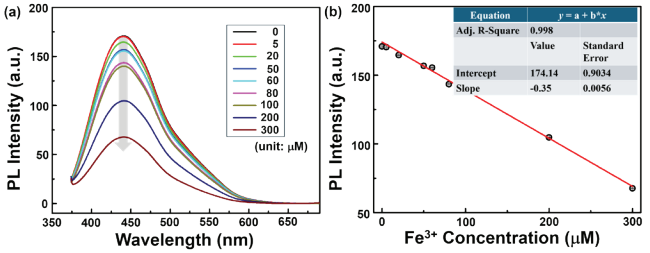

Figure 9: Fluorescence sensing performance of the bracken-derived CQDs toward Fe^{3+} ions. (a) PL emission spectra of the CQDs (0.1 mg/mL) in the presence of various Fe^{3+} concentrations ranging from 0 to 300 μM. (b) Linear calibration plot of PL intensity versus Fe^{3+} concentration. This result displays that PL excited at 360 nm showed a gradual decrease in emission intensity at 440 nm as the Fe^{3+} concentration increased.

Metal Ion Sensing Properties:

In general, Fe(III) ions induce interparticle crosslinking/aggregation through mono- or bidentate chelation with carboxylate (–COO^-) groups present on the surface of the CQDs. For the principal dopant nitrogen (N), monodentate coordination can occur *via* –NH_2; moreover, cooperative interactions between NH_2 and –COO^-/C=O groups can lead to the formation of mixed O,N-chelation complexes.[30,31] Additionally, for trace sulfur doping, –SO_x can strongly coordinate with Fe^{3+}, and adjacent –S– together with –COO^-/–OH can bind simultaneously to produce multidentate chelates.[32] In the phosphorus-doped regions, bidentate coordination (two O atoms binding to a single Fe^{3+}) is also feasible.

Based on these various coordination possibilities, the concentration dependence of adsorption was investigated by monitoring PL attenuation of a CQD solution (0.1 mg/mL) upon exposure to Fe^{3+} over 5–300 μM (Figure 9a). As the Fe^{3+} concentration increased, PL excited at 360 nm showed a gradual decrease in emission intensity at 440 nm. As shown in Figure 9b, a linear calibration curve, y = –0.35x + 174.14, obtained over 5–300 μM yielded a sensitivity of 0.35 $I_{PL/\mu M}$ and an R^2 of 0.998. Using this calibration, the limit of detection (LOD) and limit of quantitation (LOQ) were calculated as 3.3 ($S/|m|$) and 10 ($S/|m|$), respectively, where S is the standard deviation of the y-intercept and $|m|$ is the slope of the regression line.[33] The corresponding values were 8.52 μM for LOD and 25.80 μM for LOQ.

DOI: 10.36838/IJHSR816.129

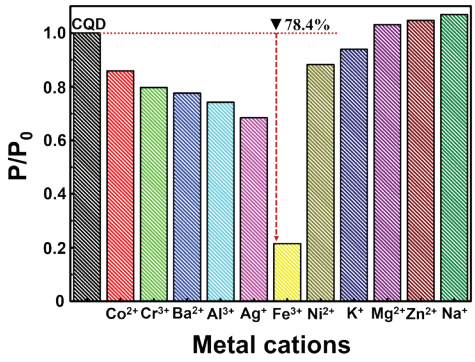

Figure 10: Selectivity evaluation of the bracken-derived CQDs toward various metal ions. The bar chart displays the relative PL intensity (P/P_0) in the presence of different metal ions (0.5 mM). PL intensity at λ_{em} = 440 nm was collected under UV light (λ_{ex} = 360 nm) after the adsorption of each metal ion in CQD solutions (0.1 mg/mL). This result suggests that Fe^{3+} ions induced a distinct fluorescent quenching effect compared to other metal ions.

Specific oxygen-containing functional groups on the surface of CQDs can serve as selective coordination sites for transition-metal ions, making them promising candidates for ion detection. As shown in Figure 10, to investigate PL intensity changes caused by metal ion adsorption, a doped CQD aqueous solution (0.1 mg/mL) was prepared, and various metal ions (0.5 mM) — Co^{2+}, Cr^{3+}, Ba^{2+}, Al^{3+}, Ag^{+}, Fe^{3+}, Ni^{2+}, K^{+}, Mg^{2+}, Zn^{2+}, and Na^{+} — were introduced to evaluate selective adsorption behavior. Among them, Fe^{3+} ions induced a distinct fluorescent quenching effect compared to other metal ions. Specifically, the PL intensity decreased by approximately 78.4% relative to the baseline of the CQDs upon Fe^{3+} adsorption. In contrast, the PL responses for Co^{2+}, Cr^{3+}, Ba^{2+}, Al^{3+}, Ag^{+}, Ni^{2+}, and K^{+} ions remained within the range of 68–88% of the initial value. Furthermore, in the presence of Mg^{2+}, Zn^{2+}, and Na^{+} ions, the PL intensity exhibited almost no change, indicating that the synthesized CQDs were not affected by the adsorption of these ions.

■ Conclusion

In this study, we successfully synthesized N, S, and P-co-doped CQDs *via* a facile hydrothermal route, using bracken, an abundant biomass, as a green carbon precursor and sulfanilamide as a dopant. The structural analyses (TEM, XRD, XPS, and FT-IR) confirmed that the CQDs possess a graphitic core with an average diameter of 9.30 nm and are rich in hydrophilic surface functional groups (–COOH and –OH) and heteroatoms (N, S, and P). These surface states endowed the CQDs with excellent water solubility and stable blue PL centered at 451 nm. The CQDs exhibited remarkable stability against high ionic strength and long-term UV irradiation, highlighting their suitability for practical sensing applications. Notably, the CQD-based sensor exhibits stable and high sensitivity within the pH range of 5.30–7.75. This range is particularly significant as it encompasses the physiological pH of biological fluids and the typical pH levels found in natural water bodies. The ability to detect Fe^{3+} within this near-neutral window without extensive pH adjustment highlights the practical utility of the proposed probe for real-time environmental monitoring and bio-analytical applications. In sensing experiments, the CQDs demonstrated high selectivity and sensitivity toward Fe^{3+}, attributed to strong fluorescent quenching induced by Fe^{3+} coordination to surface carboxyl, amine, and doped functional groups. The sensor showed a wide linear response range of 5–300 μM with the LOD of 8.52 μM. Despite these promising results, a current limitation of this study is the relatively low QY (0.03%), which may restrict the sensor's performance in environments with high optical background noise. To address this, our future research will focus on optimizing the hydrothermal reaction parameters and exploring advanced surface passivation techniques to enhance the radiative recombination rate. Furthermore, validation in complex environmental matrices, such as tap and river water, remains a priority to assess the practical robustness of the probe. Consequently, this work suggests that converting bracken into functional CQDs is a promising, eco-friendly strategy for developing low-cost fluorescent probes for environmental monitoring of heavy metal ions.

■ Acknowledgments

We thank our parents for their financial support and Dr. Jin Chul Yang for research advice.

■ References

1. Yao, C.; Yang, Y.; Li, C.; Shen, Z.; Li, J.; Mei, N.; Luo, C.; Wang, Y.; Zhang, C.; Wang, D. Heavy Metal Pollution in Agricultural Soils from Surrounding Industries with Low Emissions: Assessing Contamination Levels and Sources. *Sci. Total Environ*. **2024**, *917*, 170610. DOI: 10.1016/j.scitotenv.2024.170610.
2. Ondrasek, G.; Shepherd, J.; Rathod, S.; Dharavath, R.; Rashid, M.I.; Brtnicky, M.; Shahid, M.S.; Horvatinec, J.; Rengel, Z. Metal Contamination – A Global Environmental Issue: Sources, Implications & Advances in Mitigation. *RSC Adv*. **2025**, *15*, 3904–3927. DOI: 10.1039/D4RA04639K.
3. Li, Q.; Wang, Y.; Li, Y.; Li, L.; Tang, M.; Hu, W.; Chen, L.; Ai, S. Speciation of Heavy Metals in Soils and Their Immobilization at Micro-Scale Interfaces among Diverse Soil Components. *Sci. Total Environ*. **2022**, *825*, 153862. DOI: 10.1016/j.scitotenv.2022.153862.
4. Briffa, J.; Sinagra, E.; Blundell, R. Heavy Metal Pollution in the Environment and Their Toxicological Effects on Humans. *Heliyon* **2020**, *6*, e04691. DOI: 10.1016/j.heliyon.2020.e04691.
5. Zareh, M.M.; El-Sayed, A.S.; El-Hady, D.M. Biosorption Removal of Iron from Water by *Aspergillus niger*. *npj Clean Water* **2022**, *5*, 58. DOI: 10.1038/s41545-022-00201-1.
6. Santana-Casiano, J.M.; González-Dávila, M.; Millero, F.J. Oxidation of Nanomolar Levels of Fe(II) with Oxygen in Natural Waters. *Environ. Sci. Technol.* **2005**, *39* (7), 2073–2079. DOI: 10.1021/es049748y.
7. Fhoula, M.; Kchaou, I.; Hernández-Álvarez, C.; Dammak, M.; Boufi, S.; Martín, I.R. Highly Photoluminescent Carbon Dots: A Multifunctional Platform for pH Sensing, Nano Thermometry, and Mercury(II) Detection. *Mater. Adv.*, **2025**, *6*, 4325–4336. DOI: 10.1039/D5MA00250H.
8. Nguyen, T.-Q.; Trentin, A. Current Advances in Quantum Dots (QDs) and Carbon Dots (CDs) as Fluorescent Probes for Corrosion Detection and Biofouling Monitoring. *Mater. Today Commun.* **2025**, *47*, 113204. DOI: 10.1016/j.mtcomm.2025.113204.

9. Dhariwal, J.; Rao, G.K.; Vaya, D. Recent Advancements towards the Green Synthesis of Carbon Quantum Dots as an Innovative and Eco-friendly Solution for Metal Ion Sensing and Monitoring. *RSC Sustainability*, **2024**, *2*, 11–36. DOI: 10.1039/D3SU00375B.
10. Li, R.; Yue, J.; Zhu, F.; Zhou, J.; Liu, X. Application Progress of Carbon Quantum Dot Composites in Fluorescent Detection of Food Safety. *J. Food Sci.* **2025**, *90* (5), e70299. DOI: 10.1111/1750-3841.70299.
11. Khandaker, T.; Islam, T.; Nandi, A.; Anik, M.A.A.M.; Hossain, M.S.; Hasan, M.K.; Hossain, M.S. Biomass-Derived Carbon Materials for Sustainable Energy Applications: A Comprehensive Review. *Sustain. Energy Fuels* **2025**, *9*, 693–723. DOI: 10.1039/D4SE01393J.
12. Elugoke, S.E.; Uwaya, G.E.; Quadri, T.W.; Ebenso, E.E. Carbon Quantum Dots: Basics, Properties, and Fundamentals. *ACS Symposium Series (Chapter 1)* **2024**, *1465*, 3–42 DOI: 10.1021/bk-2024-1465.ch001.
13. Cai, D.; Zhong, X.; Xu, L.; Xiong, Y.; Deng, W.; Zou, G.; Hou, H.; Ji, X. Biomass-Derived Carbon Dots: Synthesis, Modification and Application in Batteries. *Chem. Sci.* **2025**, *16*, 4937–4970. DOI: 10.1039/D4SC08659G.
14. Nguyen, D.H.H.; Muthu, A.; Elsakhawy, T.; Sheta, M.H.; Abdalla, N.; El-Ramady, H.; Prokisch, J. Carbon Nanodots-Based Sensors: A Promising Tool for Detecting and Monitoring Toxic Compounds. *Nanomaterials* **2025**, *15* (10), 725. DOI: 10.3390/nano15100725.
15. Hemmati, A.; Emadi, H.; Nabavi, S.R. Green Synthesis of Sulfur- and Nitrogen-Doped Carbon Quantum Dots for Determination of L-DOPA Using Fluorescence Spectroscopy and a Smartphone-Based Fluorimeter. *ACS Omega* **2023**, *8* (23), 20987–20999. DOI: 10.1021/acsomega.3c01795.
16. Tavan, M.; Yousefian, Z.; Bakhtiar, Z.; Rahmandoust, M.; Mirjalili, M.H. Carbon Quantum Dots: Multifunctional Fluorescent Nanomaterials for Sustainable Advances in Biomedicine and Agriculture. *Ind. Crop. Pro*d. **2025**, *231*, 121207. DOI: 10.1016/j.indcrop.2025.121207.
17. Ding, S.; Gao, Y.; Ni, B.; Yang, X. Green Synthesis of Biomass-Derived Carbon Quantum Dots as Fluorescent Probe for Fe^{3+} Detection. *Inorg. Chem. Commun*. **2021**, *130*, 108636. DOI: 10.1016/j.inoche.2021.108636.
18. Qi, H.; Teng, M.; Liu, M.; Liu, S.; Li, J.; Yu, H.; Teng, C.; Huang, Z.; Liu, H.; Shao, Q.; Umar, A.; Ding, T.; Gao, Q.; Guo, Z. Biomass-Derived Nitrogen-Doped Carbon Quantum Dots: Highly Selective Fluorescent Probe for Detecting Fe^{3+} ions and Tetracyclines. *J. Colloid Interface Sci.* **2019**, *539*, 332–341. DOI:10.1016/j.jcis.2018.12.047.
19. Leng, L.; Liu, R.; Xu, S.; Mohamed, B.A.; Yang, Z.; Hu, Y.; Chen, J.; Zhao, S.; Wu, Z.; Peng, H.; Li, H.; Li, H. An Overview of Sulfur-Functional Groups in Biochar from Pyrolysis of Biomass. *J. Environ. Chem. Eng*. **2022**, *10* (2), 107185. DOI: 10.1016/j.jece.2022.107185.
20. Yadav, A.; Yadav, R.; Lahariya, V.; Singh, A.K. Versatile P-Doped Carbon Quantum Dots Derived from Green Precursor: An Efficient Metal Ion Sensor and Photocatalytic Behaviour in Aqueous Environment. *Res. Chem. Intermed*. **2024**, *50*, 1873–1893. DOI: 10.1007/s11164-023-05225-x.
21. Mohandoss, S.; Ganesan, S.; Palanisamy, S.; You, S.G.; Velsankar, K.; Sudhahar, S.; Lo, H.-M.; Lee, Y.R. Nitrogen, Sulfur, and Phosphorus Co-doped Carbon Dots-Based Ratiometric Chemosensor for Highly Selective Sequential Detection of Al^{3+} and Fe^{3+} ions in Logic Gate, Cell Imaging, and Real Sample Analysis. *Chemosphere* **2023**, *313*, 137444. DOI: 10.1016/j.chemosphere.2022.137444.
22. Ebuele, V.O.; Santoro, A.; Thoss, V. Phosphorus Speciation by ^{31}P NMR Spectroscopy in Bracken (*Pteridium aquilinum* (L.) Kuhn) and Bluebell (*Hyacinthoides non-scripta* (L.) Chouard ex Rothm.) Dominated Semi-natural Upland Soil. *Sci. Total Environ.* **2016**, 566–567, 1318–1328. DOI: 10.1016/j.scitotenv.2016.05.192.
23. Pei, S.; Wang, Y.; Cai, S.; Yan, K.; Luo, K.; Ma, Y. Synthesis of Sulfur-Doped Carbon Quantum Dots from *Solanum Nigrum* for Ciprofloxacin Detection in Yogurt Samples and Antibacterial Activity. *RSC Adv.* **2025**, *15*, 27294–27299 DOI: 10.1039/D5RA04505C.
24. Nair, S.S.P.; Kottam, N.; Kumar, P.S.G. Green Synthesized Luminescent Carbon Nanodots for the Sensing Application of Fe^{3+} Ions. *J. Fluoresc.* **2020**, *30*, 357–363. DOI: 10.1007/s10895-020-02505-2.
25. Solayman, H.M.; Leong, K.H.; Hossain, M.K.; Khan, M.B.; Kang, K.; Jiang, J.-J.; Aziz, A.A. Carbon Quantum Dots: Comparative Analysis of Synthesis Strategies and Their Environmental Application. *Next Materials* **2025**, *8*, 100787. DOI: 10.1016/j.nxmate.2025.100787.
26. Singh, A.; Qu, Z.; Sharma, A.; Singh, M.; Tse, B.; Ostrikov, K.; Popat, A.; Sonar, P.; Kumeria, T. Ultra-Bright Green Carbon Dots with Excitation-Independent Fluorescence for Bioimaging. *J. Nanostruct. Chem.* **2023**, *13*, 377–387. DOI: 10.1007/s40097-022-00501-5.
27. Ding, H.; Li, X.-H.; Chen, X.-B.; Wei, J.-S.; Li, X.-B.; Xiong, H.-M. Surface States of Carbon Dots and Their Influences on Luminescence. *J. Appl. Phys.* **2020**, *127*, 231101. DOI: 10.1063/1.5143819.
28. Masaeli, E.; Das, P.; Srinivasan, S.; Rajabzadeh, A.R. Carbon Dot-Based Mechanofluorescent Hydrogel with Tunable Fluorescence for Bioengineering Applications. *Small* **2026**, Early View (Online Version) e12265 DOI: 10.1002/smll.202512265.
29. Dua, S.; Kumar, P.; Pani, B.; Kaur, A.; Khanna, M.; Bhatt, G. Stability of Carbon Quantum Dots: A Critical Review. *RSC Adv.* **2023**, *13*, 13845. DOI: 10.1039/D2RA07180K.
30. Li, Y.; Liu, Y.; Shang, X.; Chao, D.; Zhou, L.; Zhang, H. Highly Sensitive and Selective Detection of Fe^{3+} by Utilizing Carbon Quantum Dots as Fluorescent Probes. *Chem. Phys. Lett*. **2018**, *705*, 1–6. DOI: 10.1016/j.cplett.2018.05.048.
31. Wang, Z.; Long, P.; Feng, Y.; Qin, C.; Feng, W. Surface Passivation of Carbon Dots with Ethylene Glycol and Their High-Sensitivity to Fe^{3+}. *RSC Adv*. **2017**, *7*, 2810–2816. DOI: 10.1039/C6RA25465A.
32. Shabbir, H.; Csapó, E.; Wojnicki, M. Carbon Quantum Dots: The Role of Surface Functional Groups and Proposed Mechanisms for Metal Ion Sensing. *Inorganics* **2023**, *11* (6), 262. https://doi.org/10.3390/inorganics11060262.
33. Yamamoto, T.; Sato, K.; Yamaguchi, M.; Mitamura, K.; Taga, A. Development of Simultaneous Quantitative Analysis of Tricarboxylic Acid Cycle Metabolites to Identify Specific Metabolites in Cancer Cells by Targeted Metabolomic Approach. *Biochem. Biophys. Res. Commun*. **2021**, *584*, 53–59. DOI: 10.1016/j.bbrc.2021.10.072.

Authors

Rachel Jiwon Park, an 11th-grade student at Branksome Hall Asia in Jeju, Republic of Korea, is deeply committed to exploring the frontiers of biochemistry and genetic engineering. Her academic pursuits are deeply rooted in a profound commitment to global public health, with a specialized focus on developing diagnostic and preventive frameworks against emerging pathological threats. By addressing critical global health disparities through rigorous scientific inquiry, she aspires to facilitate cross-border scientific breakthroughs that

DOI: 10.36838/IJHSR816.129

safeguard human life and enhance the resilience of international society.

Hailey Jeongwon Park is a Grade 9 student at Branksome Hall Asia in Jeju, Republic of Korea. While maintaining a strong foundation in science, she plans to major in Business with a specific focus on bridging the gap between scientific innovation and commercial viability. Driven by her experience in developing science-based inventions, she is deeply interested in designing sustainable business models that can bring laboratory research to the real-world market.